Desalination and Water Treatment
www.deswater.com
doi: 10.5004/dwt.2023.29710

302 (2023) 43–52
August

Effect of organic foulants on ions separation at different ionic strengths in a nanofiltration system

Fang Gao[a], Xiaofei Xue[a,*], Lin Ma[b,*], Lingyun Li[a], Jianhua Mao[a], Yanwei Shi[a], Xiaoyan Yao[a]

[a]*Beijing Enterprises Water Group (China) Investment Limited, BEWG Building, Poly International Plaza T3, Zone 7, Wangjingdongyuan, Chaoyang District, Beijing 100102, China, emails: xuexiaofei@bewg.net.cn (X. Xue), gaofang@bewg.net.cn (F. Gao), lilingyun@bewg.net.cn (L. Li), maojianhua@bewg.net.cn (J. Mao), shiyanwei@bewg.net.cn (Y. Shi), yaoxiaoyan@bewg.net.cn (X. Yao)*
[b]*Beijing TDR ENVIRON-TECH Corporation Limited, Beijing 100176, China, email: 245113039@qq.com*

Received 26 December 2022; Accepted 12 June 2023

ABSTRACT

This study aimed to present the fouling behavior of nanofiltration membrane in homogeneous organic foulants and heterogeneous organic foulants, using the modified extended Derjaguin–Landau–Verwey–Overbeek theory. It found that homogeneous organic foulants (e.g., humic acid and bovine serum albumin) became more problematic with increasing ionic strength. Conversely, the permeate reduction from heterogeneous organic foulants (BSA-HA) intensified and then lightened. Significantly, it also explored the effectiveness of nanofiltration for separating NaCl and Na_2SO_4 ions, focusing on the impact of ionic strength and organic fouling on ion separation. Our results show that ion separation increased from 11.08 to 84.2 as the interaction energy between the foulant and the virgin membrane improved from –13.9 ± 0.5 mJ/m^2 to –35.6 ± 2.4 mJ/m^2 in the initial stage (virgin membranes). This increase in separation is due to the Donnan-like effect caused by negatively charged dissolved substances. However, ion separation gradually reduced as interfacial energy between the organics and fouled membrane decreased. This reduction can be attributed to cake-enhanced concentration polarization and weakened electrostatic repulsive forces.

Keywords: Ion separation; Nanofiltration; Organic fouling; Derjaguin–Landau–Verwey–Overbeek theory; Donnan-like effect

1. Introduction

In today's world, water resources are declining and the quality of potable water is gradually improving, the membrane industry's traditional sector and resource recovery constitute a significant portion of its global turnover [1–3]. Over the past decade, China has mandated zero discharge of wastewater in industries such as coal and petrochemicals. Additionally, the mixed salts present in the wastewater are categorized as hazardous waste. However, monovalent and polyvalent salts such as NaCl and Na_2SO_4 can be recovered as valuable resources by isolating them from the mixed solution [4]. Compared to mechanical vapor recompression (MVR) or electrodialysis of mixed salt, nanofiltration (NF) offers several advantages such as low-carbon operation and high separation efficiency [5,6].

Previous studies on NF processes have shown that its ability to effectively reject multivalent salt while allowing monovalent salt to pass through makes it suitable for water softening, desulfurization wastewater treatment, and lithium separation from brine solutions [7–9]. As the number of applications for NF increases steadily, research efforts are focused on using NF membranes to efficiently separate target substances and economically recover them. Studies have also investigated the effect of different types of ions

* Corresponding authors.

and solution pH on membrane permeability and the selective rejection of multivalent cations [10,11]. Furthermore, researchers have investigated the significant increase in selectivity of mono- and multivalent cations in weakly acidic hydrochloric solutions [12]. Various studies have reported the effect of cation valence on the selective rejection of monovalent and multivalent ions due to complex mechanisms involving steric hindrance, electrostatic screening, and Donnan effects [13–15].

Additionally, humic acid (HA) representing natural organic matter (NOM) was used to investigate the role of chemical and physical interactions in NOM fouling of NF membranes [16]. The researchers reported that membrane fouling worsened as electrolyte concentration increased due to humic acid absorption onto the hydrophilic membrane surface. Moreover, they investigated various mathematical models to determine the kinetics and fouling mechanisms of the NF membrane. The experimental results at low ionic strength were fitted with a pore-blocking model, while those at high ionic strength followed cake formation. Additionally, for single macromolecular proteins, a similar phenomenon was observed wherein flux reductions became more significant with increasing ionic strength of the feed solution [17]. This phenomenon was attributed to an increase in ionic strength that compressed the electric double layer due to charge screening, which reduced the electrostatic repulsion among bovine serum albumin (BSA) molecules and between the BSA molecules and the membrane [18]. However, several researchers investigated the cleaning procedures of organic-fouled NF and reverse osmosis (RO) membranes using the dissolved salt solution [19,20]. In addition, experiments using a feed consisting of mixed foulants, including humic acid, proteins, and polysaccharides, showed that the poly-foulant had less severe fouling than individual foulants at high ionic strength. These studies indicated that the interaction between different foulants plays a more critical role than the interactions within the foulants and between foulants and the membrane in a mixed foulant system [21]. Nevertheless, the quantitative effects of the interactions between foulants and membranes on the separation of hybrid salts are not yet fully understood. Moreover, the quantitative relationships between ion separation and fouling behavior in the presence of mixed foulants are still poorly studied.

This study utilized bovine serum albumin (BSA), humic acid (HA), and their mixture as organic model foulants. Additionally, dissolved inorganic substances (NaCl and Na_2SO_4) were used as targeted ions, and the ionic strength was adjusted. By investigating the influence of ionic strength on interactions between single/mixed foulants and the membrane, including van der Waals (LW) and acid–basic (AB) interactions, the changes in three membrane fouling contributors were used to investigate the factors and mechanisms that caused NF membrane fouling. Furthermore, the quantitative relationships between the separation of mixed salts and different foulants and their fouling behavior were studied.

2. Materials and methods

2.1. Chemicals and membrane

Two organic substances, bovine serum albumin (BSA, Sigma-Aldrich A1933, ≥98% purity Sigma-Aldrich, USA) and humic acid (HA, Sigma-Aldrich 53680, USA), were used as model foulants in this study. Single foulant systems (HA and BSA alone) and hybrid foulant systems, where equal amounts of BSA and HA were dissolved, were used to investigate the influence of their fouling behaviors and ionic strength on ion separation. Zeta potential values of single and mixed foulants in the feed solution were measured using a Zetasizer Nano ZS (Beckman Coulter, Inc., USA) and are presented in Table 1. Sodium chloride and sodium sulfate (AR reagent, China) were used as the inorganic ion sources. The ion concentrations (Cl^- and SO_4^{2-} ions) in the experiments were 5:5, 20:20, and 50:50 mM, corresponding to salt concentrations of 5,021; 20,050 and 50,125 mg/L. The experiments were conducted using three different solutions: the feed solution, which consisted of a mixture of foulants and inorganic ions; the primary concentrated solution of coal gasification wastewater, which was processed by reverse osmosis; and the evaporated solution.

The pH value of all feed and test solutions was maintained at 7.0 ± 0.3. Unless otherwise specified, all reagents and chemicals used in the study were of analytical grade. Ultrapure water (Milli Q, with a resistivity of 18.2 MΩ) was used to prepare working solutions. Commercial nanofiltration membranes (GL by GE Osmonics, Inc., US) were used to investigate ion separation and fouling behavior over a range of ion concentrations. The negatively charged membrane used in the study was selected for its high permeate flux and superior ion separation performance.

2.2. Membrane surface morphology and contact angle

The membrane surface morphology of virgin and fouled PA membranes was measured by scanning electron microscopy (SEM; JSM–7610F, JEOL Ltd., Japan) to determine the filter cake structure and how variant properties influenced the filter cake caused by the filter cake single or mixed foulant. All samples were completely dried in clean plastic boxes at room temperature and were imaged by an accelerating voltage of 20 kV. To prepare the samples for SEM imaging, the samples surfaces were coated by a thin layer of gold-palladium based on a sputter coating method. Specifically, the sputter coating was conducted at a current of 15 mA for 90 s. The contact angles (θ) of the virgin and fouled membranes were measured using a contact angle goniometer (K100, Kruss, Germany) through the sessile drop technique. BSA, HA, and BSA-HA foulants were used to prepare fouling lawns on a non-porous RO membrane to achieve complete coverage through dead-end filtration. The contact angle was measured using three different probe liquids with known surface tension values, typically water, ethylene glycol, and diiodomethane. This enabled the surface tensions between the foulants and the virgin/fouled PA membranes to be obtained.

Table 1
Zeta potential of single and mixed foulants

pH	Zeta potential of foulants (mV)		
	BSA	HA	BSA + HA
7.0 ± 0.3	–6.9	–27.2	–21.5

2.3. Nanofiltration

NF experiments were conducted using a laboratory-scale cross-flow membrane filtration system equipped with a rectangular membrane module with an area of 40 cm^2 (Fig. 1). To transport the feed solution, a gear pump (WT3000-1JB-A, Longer Pump, China) was used, and the flow was adjusted accordingly. The applied pressure was controlled using a needle valve and monitored using pressure transmitters (SSI Technologies, Inc. 0–25 bar, China). The permeate flux was measured using an electronic balance (Ohaus Instruments Co., Ltd., China) and recorded using a computer data logging system. During filtration, the permeation and retention were recycled back to the feed tank at stated intervals. For each filtration test, a new membrane was immersed in ultrapure water and compacted with pure water for 2 h to ensure stable permeate flux. The test duration was approximately 20 h, or until the desired permeate flux reduction was achieved. The chloride and sulfate ion concentration in the initial and final permeates over 20 h of fouling test, as well as the corresponding feed, were measured by ion chromatography (Dionex-550, USA). Each condition was tested with at least two replicates. Throughout the experiment, variant foulant systems (total organic foulant concentration of 20 mg/L, single foulant: 20 mg/L BSA and HA; mixed foulant: 10 mg/L BSA and 10 mg/L HA), anionic strength range of 10–100 mM (molar concentration of NaCl and Na_2SO_4 was 5, 20, and 50 mM, respectively), and cation composition (Na^+ system) were investigated. The conditions included an applied pressure of 5 bar and a temperature of 293 K for the entire experiment.

Anion rejection, r, is calculated using Eq. (1), where c_p and c_f are ion concentrations in the permeate and the feed.

$$r(\%) = \frac{c_f - c_p}{c_f} \times 100 \tag{1}$$

The separation between Cl^- and SO_4^{2-}, S, which can be expressed in terms of rejection at the corresponding ion, is defined by Eq. (2).

$$S = \frac{c_{Cl^-,p}}{c_{Cl^-,f}} \times \frac{c_{SO_4^{2-},f}}{c_{SO_4^{2-},p}} = \frac{100 - r_{Cl^-}}{100 - r_{SO_4^{2-}}} \tag{2}$$

$$\mathrm{DIS} = S_0 - S_{20} \tag{3}$$

where S_0 is defined as the separation of multi-ion by a virgin membrane at the initial stage of the test. S_{20} is the separation of multi-ions by a fouled membrane at the final stage of the test. DIS is the corresponding separation differences over 20 h.

2.4. Theory

Interfacial free energies can be obtained through contact angle (θ) measurements between a liquid and a membrane surface or foulants lawn. In this experiment, contact angle measurements were performed using a variety of probe liquids, including ethylene glycol and diiodomethane, but the most significant modification involved the use of a water probe with different ionic strengths ranging from 10 to 100 mM.

The extended Young–Dupré equation:

$$\left(1 + \cos\theta\right)\gamma_l^T = 2\left(\sqrt{\gamma_m^{LW}\gamma_l^{LW}} + \sqrt{\gamma_m^+\gamma_l^-} + \sqrt{\gamma_m^-\gamma_l^+}\right) \tag{4}$$

where γ^T, γ^{LW}, γ^+ and γ^- are total liquid surface tension, Lifshitz–van der Waal (LW), electron–donor, and electron–acceptor components of the solid surface tension, respectively.

γ^{TOT} is the total surface tension of a pure substance obtained as a sum of LW and AB components, yielding:

$$\gamma^{TOT} = \gamma^{LW} + \gamma^{AB} \tag{5}$$

And the acid–base component, AB, is given by:

$$\gamma^{AB} = 2\sqrt{\gamma^+\gamma^-} \tag{6}$$

The interaction energy between the foulants and membrane surfaces can be described using Derjaguin–Landau–Verwey–Overbeek (M-XDLVO) theory as a sum of Liftshitz-van der Waals and Lewis acid–base interactions [22]:

$$\Delta G_{mlf}^T = \Delta G_{mlf}^{LW} + \Delta G_{mlf}^{AB} \tag{7}$$

The Lifshitz–van der Waals and Lewis acid–base interfacial free energy component, ΔG_{mlf}^{LW} and ΔG_{mlf}^{AB} of the XDLVO equation may then be written as respectively

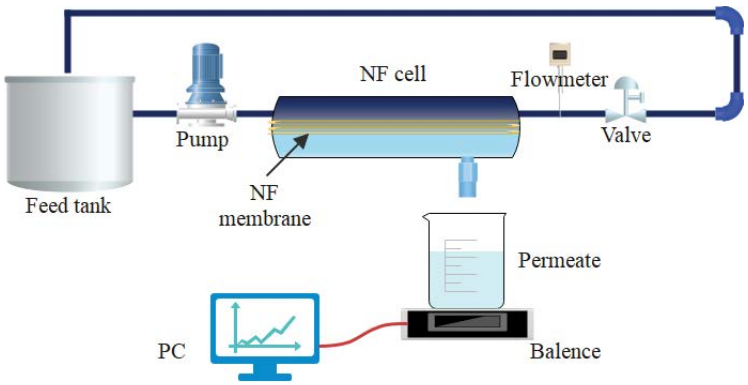

Fig. 1. Schematic diagram of the cross-flow nanofiltration system.

$$\Delta G_{\mathrm{mlf}}^{\mathrm{LW}} = 2\left(\sqrt{\gamma_l^{\mathrm{LW}}} - \sqrt{\gamma_m^{\mathrm{LW}}}\right)\left(\sqrt{\gamma_f^{\mathrm{LW}}} - \sqrt{\gamma_l^{\mathrm{LW}}}\right) \quad (8)$$

$$\begin{aligned}\Delta G_{\mathrm{mlf}}^{\mathrm{AB}} = {} & 2\sqrt{\gamma_l^+}\left(\sqrt{\gamma_m^-} + \sqrt{\gamma_f^-} - \sqrt{\gamma_l^-}\right) \\ & + 2\sqrt{\gamma_l^-}\left(\sqrt{\gamma_m^+} + \sqrt{\gamma_f^+} - \sqrt{\gamma_l^+}\right) \\ & - 2\left(\sqrt{\gamma_f^-\gamma_m^+} + \sqrt{\gamma_f^+\gamma_m^-}\right)\end{aligned} \quad (9)$$

where the subscript (m) is the virgin/fouled membrane, (f) denotes the mixed foulant, and (l) refers to the solution.

3. Results and discussion

3.1. Effect of ionic strength on permeate flux and fouling behavior

Fig. 2 illustrates the impact of ionic strength on the initial permeate flux of single and mixed foulant systems. As the ionic strength of the feed increased, the initial permeate flux of both single systems (BSA and HA alone) and the hybrid system (BSA-HA) by the fresh NF membrane decreased due to concentration-enhanced osmotic pressure. Notably, in the first 3 h, there were insignificant reductions in flux for both single and mixed foulant systems. It is worth noting that the trends observed in this study for single and mixed systems were contrary to those reported in the literature for dead-end filtration. In previous investigations, the flux decreased rapidly, with the most substantial reduction occurring at the initial fouling stage due to the organic foulant cake's quick formation on the membrane during dead-end filtration. However, in the case of cross-flow filtration, which is dominant in the nanofiltration process, relatively hydrophobic organic foulants do not readily adsorb on the membrane surface, which is composed of hydrophilic materials at the initial stage [23]. During the fouling tests, different fouling behaviors were observed for the corresponding foulants. As shown in Fig. 2a, for a single protein, an increase in ionic strength can lead to more severe fouling, as observed for the BSA system, where the normalized flux decreased to 78.5% at 50:50 mM, 79.1% at 20:20 mM, and 88.4% at 5:5 mM over 20 h of fouling tests. On the other hand, for a single organic acid, the effect of ionic strength on the fouling behavior of HA was minor, and the ultimate flux losses first increased and then decreased within the ionic strength range of 5:5–50:50 mM. The most severe fouling was observed at 20:20 mM, according to Fig. 2b. Higher ionic strength may weaken the electrostatic repulsive forces between BSA (or HA) molecules by the electrical double layer compression effect, considering the same structure and charge between homogeneous molecules.

The fouling behavior was found to be much more severe at lower ionic strengths of 5:5 and 20:20 mM. After 5 h, the flux decline rates accelerated, and reductions were 31.6% and 20.5%, respectively, over the 20-h fouling test. These results suggest that the electrostatic repulsive forces between BSA and HA are suppressed by adequate ion concentration in the feed, considering that both BSA and HA molecules have the same charge. As a result, the compressed electrical double layer (EDL) can facilitate the formation of aggregates between BSA and HA monomers. However, at an ionic

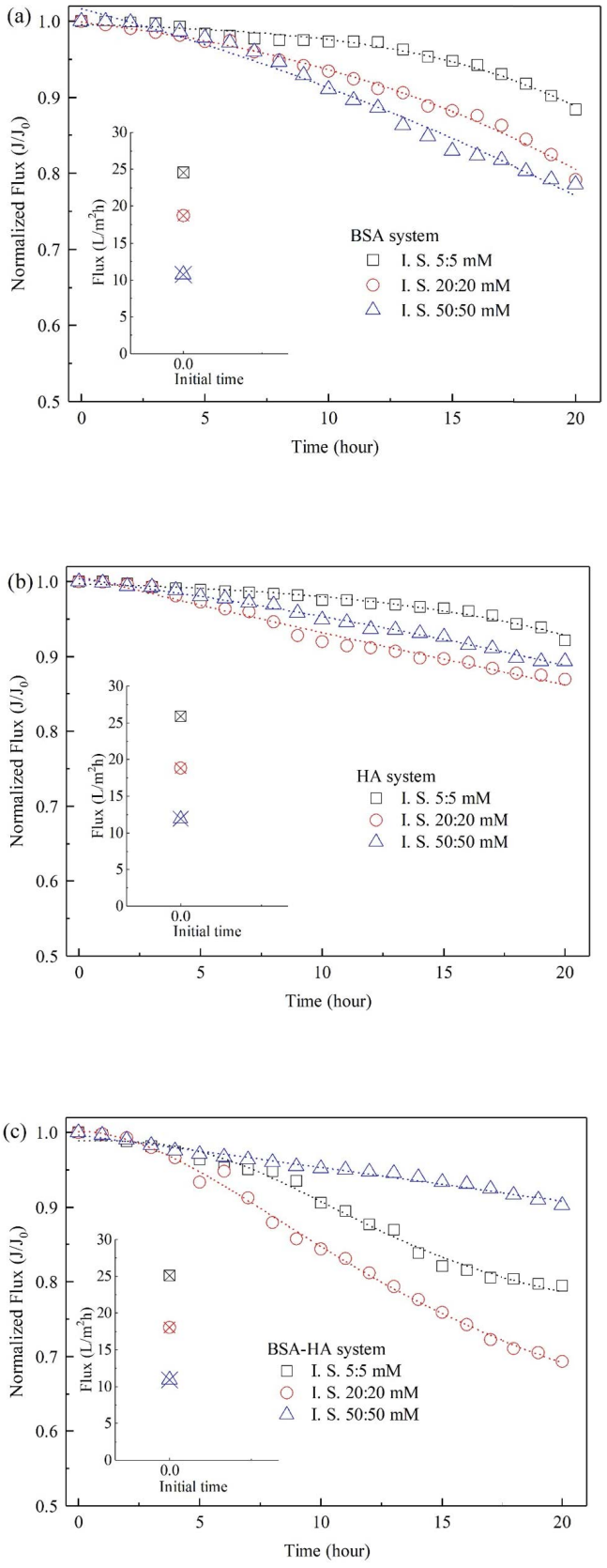

Fig. 2. Effect of ionic strength on permeate flux and fouling behaviors: (a) BSA system, (b) HA system, and (c) BSA-HA system.

strength of 50:50 mM, the flux loss was only 9.7% fouling degree, indicating that the effect of electrostatic repulsion was weakened. Not only did the more substantial EDL compression effect by electrostatic repulsion between HA and BSA caused by strong ionic strength, but it also enhanced the distance between molecules and thus hindered molecular interaction, for example, amino and carboxyl or hydroxyl groups [17,19]. Part c of Fig. 2 further implies that a hybrid BSA-HA system in the feed at 50:50mM was formed by BSA and HA monomers, with the flux reduction functions of HA and BSA systems.

3.2. Effect of ionic strength and fouling behavior on ions rejection

In Fig. 3, the influence of ionic strength on the rejection of Cl^- and SO_4^{2-} by the virgin membrane is presented for three organic foulant systems (BSA, HA, and BSA-HA). The initial retention rates of Cl^- were positive at low ionic strength, indicating that the NF membrane could effectively reject monovalent ions. However, as the total ion concentration increased, the Cl^- rejection declined, and in some cases, even negative values were obtained. The trend observed was Cl^- rejection (BSA) > Cl^- rejection (BSA-HA) > Cl^- rejection (HA), which can be attributed to the Donnan-like effect. On the other hand, the initial rejection of SO_4^{2-} was relatively insensitive to changes in ionic strength, as illustrated in Fig. 3a and b. This can be explained by the combined effects of the Donnan effect and ion competition, which lead to negative rejection of monovalent ions at near-neutral pH.

During the experiment, Table 2 shows that the change in fouling degree contributed to the rejection of multi-ion. Three systems demonstrated a decrease in Cl^- rejection and relatively stable SO_4^{2-} rejection. In the BSA system, Cl^- rejection reduced to 14.4%, 5.4%, or –27.5% at ion strengths of 5:5, 20:20, or 50:50 mM, respectively, over 20 h. Meanwhile, SO_4^{2-} rejection remained statistically ≥95%. A similar phenomenon was observed in the BSA-HA system, which was attributed to the weakening charge of the membrane surface and concentration polarization. The fouling cake formed by foulants adsorbed on the membrane surface, and tortuous channels within the cake layer may hinder the back diffusion of ions. The weakening electrostatic repulsive force between the fouled membrane and anions also led to more ions being deposited on the membrane surface. However, in the HA system, Fig. 3b indicates that over the 20-h fouling test at high ionic strength, the change in Cl^- and SO_4^{2-} rejections were different. The results showed that the SO_4^{2-} rejection by the fouled membrane was only 86.5%, much lower than other rejections in the BSA or BSA-HA system. This was attributed to the reinforced concentration polarization and the enhancement of the Donnan-like effect by the smaller and stronger charged HA molecules.

3.3. Characterization of NF membranes and foulants

Four types of membranes are considered in this study: virgin membrane, BSA-fouled membrane, HA-fouled membrane, and BSA-HA fouled membrane. The effect of an increase in ionic strength on these membranes is investigated. Fig. 4a shows a virgin NF membrane with a surface covered in dots due to the formation of polyamide, which

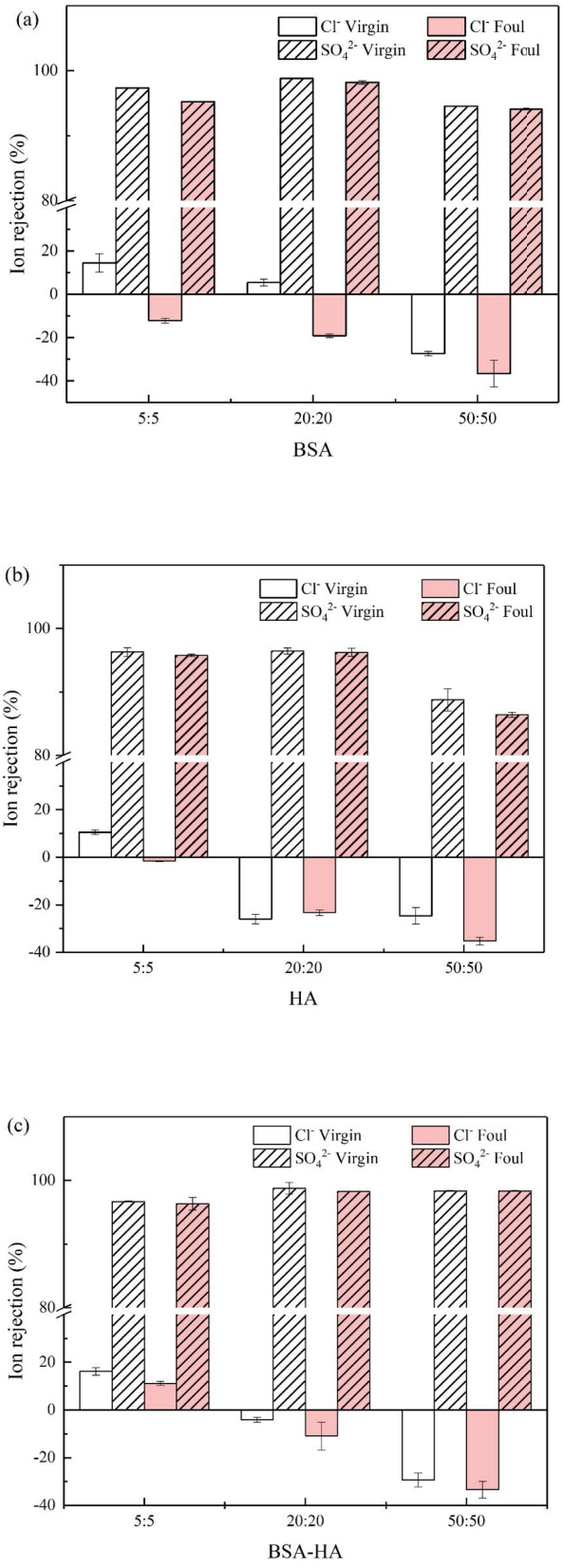

Fig. 3. Effect of ionic strength and fouling behaviors on ions rejection: (a) BSA system, (b) HA system, and (c) BSA-HA system.

Table 2
Effect of ionic strength and fouling behaviors on ions rejection: (a) BSA system, (b) HA system, (c) BSA-HA system

		5:5 mM		20:20 mM		50:50 mM	
		Cl^-	SO_4^{2-}	Cl^-	SO_4^{2-}	Cl^-	SO_4^{2-}
BSA	Virgin	14.4 ± 4.24	97.35 ± 0.07	5.4 ± 1.56	98.8 ± 0.01	–27.45 ± 1.06	94.5 ± 0.07
	Fouled	–12.2 ± 1.13	95.25 ± 0.07	–19.2 ± 0.85	98.2 ± 0.28	–36.7 ± 6.22	94.1 ± 0.14
HA	Virgin	10.55 ± 0.92	96.3 ± 0.71	–26 ± 1.97	96.5 ± 0.49	–24.7 ± 0.46	88.75 ± 1.77
	Fouled	–1.65 ± 0.21	95.8 ± 0.21	–23.3 ± 1.13	96.3 ± 0.64	–35.3 ± 1.63	86.4 ± 0.42
BSA-HA	Virgin	16.17 ± 1.54	96.7 ± 0.06	–4.12 ± 1.12	98.7 ± 0.94	–29.3 ± 2.91	98.35 ± 0.08
	Fouled	11.13 ± 0.87	96.35 ± 0.99	–10.9 ± 5.84	98.27 ± 0.04	–33.4 ± 3.44	98.3 ± 0.07

serves as an effective rejection layer [24]. SEM images in Fig. 4b–d reveal morphological changes in the BSA-fouled membranes. Except for the membrane at 5:5 mM, the surfaces of membranes at 20:20 and 50:50 mM appear smooth and covered with more BSA molecules. This leads to a more severe flux reduction at higher ionic strength, as observed in corresponding ionic strength. In HA fouling, the HA cakes within the ionic strength range were more porous and provided less resistance to permeate, as shown in Fig. 4e–f. The normalized flux in Fig. 2b confirms this finding. For mixed BSA-HA fouling, the thick and dense cake layers of mixed foulant varied with salt properties, as shown in Fig. 4h–j, resulting in a significant loss of permeate flux. Additionally, the results suggest that the structure of BSA-HA varied with ionic strength in the feed. For instance, the main structures of the foulant at 5:5 and 20:20 mM were $[BSA\text{-}HA]_n$ polymers, while those at 50:50 mM were BSA-BSA and HA-HA.

Table 3 presents the intensity size distribution and aggregation of single and mixed foulants at different ionic strengths. For the single BSA system, the size distributions ranged from 7.3 to 10.4 nm within 5:5–50:50 mM. Additionally, the size distribution of mono BSA molecules was about 3.6 nm. The results indicate that the feed contained multi-aggregates of two and three BSA particles below 50:50 mM. For the single HA system, the major peak in the size distribution was between 1.1 and 1.6 nm within the range of ionic strength. The size distribution of mono HA molecules was approximately 0.3–0.9 nm. When BSA combined with HA, the aggregation of BSA-HA was 1–2 times higher than that of BSA alone within the same range of 5:5 and 20:20 mM. However, considering the molecular size of HA, proteins wrapped with HA can hardly form the aggregation, as shown in Table 3. Therefore, the results suggest that HA can act as a bridging agent between macro-molecules (BSA).

3.4. Measured physicochemical properties between foulants and membranes

Table 4 summarizes the physicochemical properties of single and mixed foulants used in the study. Both BSA and HA exhibited a decline in water contact angles with an increase in ionic strength. This result can be explained by ion-enhanced hydration, where an increase in hydrated ions reduces the interfacial energy of water molecules, leading to improved interaction between water molecules and the surface of the organic foulant. However, for the hybrid foulant system, the peak value of water contact angle was 82.0° ± 1.4° and occurred at an ionic strength of 50 mM, which can be attributed to differences in the structure. These contact angles suggest that the hydrophilicity of different organic substances varied with the ionic strength of the solution.

Table 5 presents the measured physicochemical properties of virgin and fouled membranes, including virgin PA, BSA-fouled, HA-fouled, and BSA-HA fouled PA. The hydrophilic surface of virgin PA membrane slightly increased its contact angle with an increase in ionic strength, which could be attributed to the reducing interfacial energy of the aquatic solution. However, fouled membranes by different types of foulants had different trends of contact angles within the ionic strength range of 5:5–50:50 mM, as shown in Table 5. Water contact angles of BSA-fouled membranes increased with an increase in ionic strength, indicating a more severe fouling propensity due to more foulant mass deposited on the membrane surface. On the other hand, for the HA system, an opposite trend of changing contact angles occurred within the same range of ionic strength. This phenomenon indicated that the effect of ionic strength on the membrane fouling behavior by HA was not evident, as the electrostatic interaction between HA molecules played a dominant role over the electrical double layer compression effect by high ionic strength. The three surfaces of HA-fouled membranes in feeds with varying ionic strength exhibited similar changes, given the relatively high concentration of salt on the testing membrane sample. The weakening interfacial energy of water molecules by ion-enhanced hydration led to a decline in contact angles. Comparing contact angles and fouling behaviors of the three BSA-HA fouled membranes in the mixed foulant system, the results indicated that enhancing the ionic strength of the feed can benefit the improvement of the NF membrane anti-fouling performance for mixed foulants [25].

3.5. Interfacial free energy for permeate and ions separation

Table 6 presents the estimated interaction energy between the different foulants (BSA, HA, and BSA-HA) and the corresponding virgin or fouled membranes, as calculated using the XDLVO approach based on Eq. (7). In all cases, the interaction energy between the foulant and the virgin membrane (G^T_V) was negative, indicating that the foulants were more likely to be deposited on the membrane surface. G^T_V values initially increased and then decreased with increasing ionic strength, and this trend was more

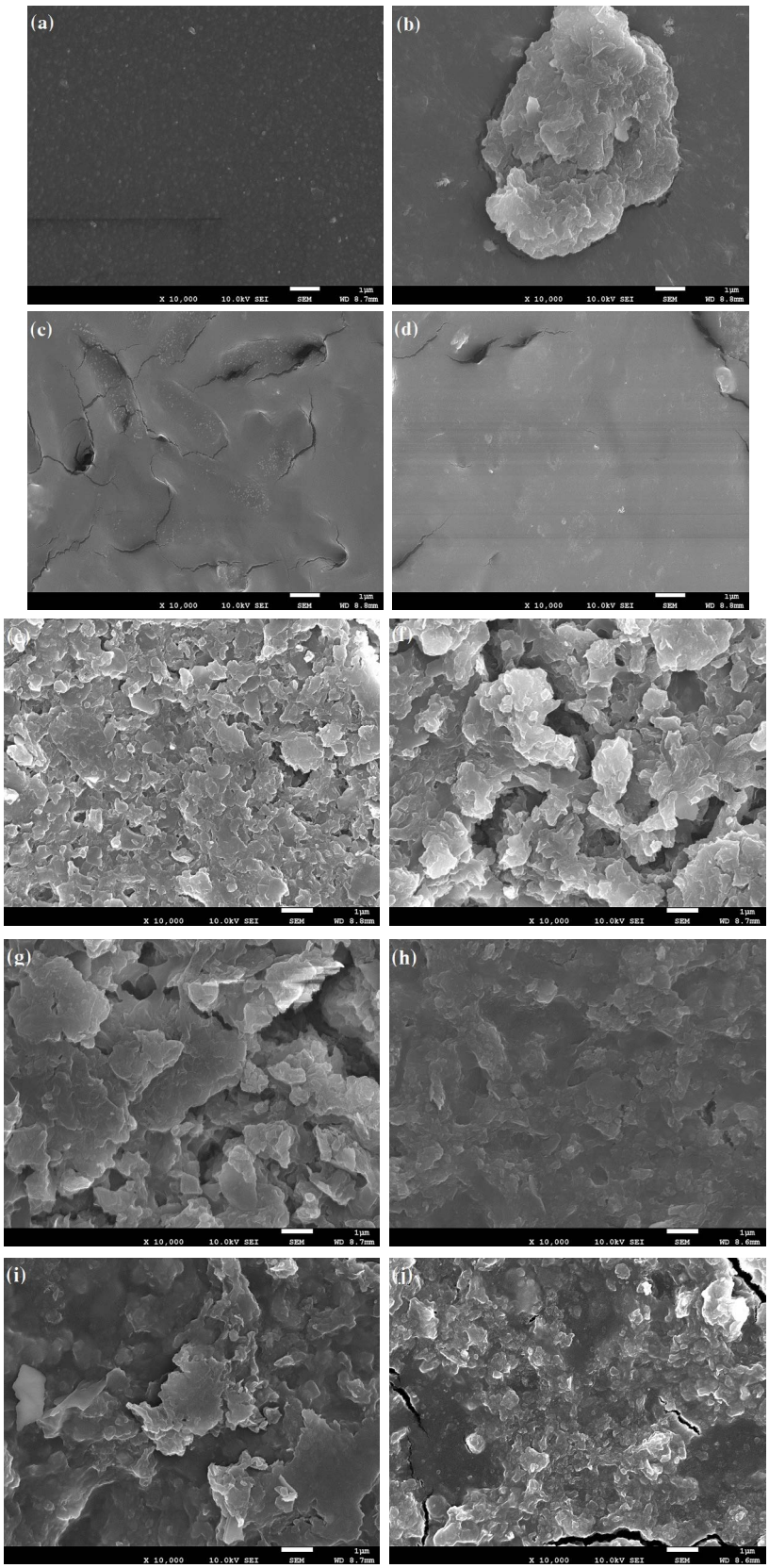

Fig. 4. Scanning electron microscopy images of NF membrane surface, (a) virgin, (b) BSA system at 5:5 mM, (c) BSA system at 20:20 mM, (d) BSA system at 50:50 mM, (e) HA system at 5:5 mM, (f) HA system at 20:20 mM, (g) HA system at 50:50 mM, (h) BSA-HA system at 5:5 mM, (i) BSA-HA system at 20:20 mM, and (j) BSA-HA system at 50:50 mM.

pronounced for the mixed system. At high feed stream ionic strength (50:50 mM), the Debye length and electric double layer (EDL) were significantly reduced, resulting in the suppression of the ordinary BSA-HA acid–basic force [26]. In addition, the G_F^T values between the foulants (BSA, HA, and BSA-HA) and the fouled membranes at different ionic strengths positively correlated with the permeate flux reduction rate (J/J_0) at the end of the fouling tests, as shown in Table 6. These results suggest that the G_F^T values could be used to predict fouling behaviors. Similar phenomena have been observed in studies on microbial cells or colloidal adhesion to membranes, where various interactions play a role [27,28].

To investigate the effect of single/mixed foulant systems on the separation of ions, the interfacial free energies between the virgin membrane surface and the foulants were calculated at different ionic strengths. The results in Fig. 5 demonstrate that the ion separation degree increases with a decrease in G_V^T values within the range of 5:5–50:50 mM. The ion separation degree increased from 24.2 to 32.3 at low ionic strength, while at moderate ionic strength, the ion separation degree was between 35.5 and 84.2, and at high ionic strength, it ranged from 11.1 to 78.4. The overall interaction energy can predict whether the nature of the interaction between the organic foulants and membrane is attractive (G_V^T is negative), providing a valuable method for predicting the number of foulants approaching the membrane surface. The presence of organic macromolecules containing carbonyl and carboxyl groups, similar to SO_4^{2-} ions, can compete with inorganic Cl^- ions, weakening the electrostatic repulsive force between membrane surfaces via the Donnan effect [29]. The smaller steric structure and weaker charge of Cl^- ions significantly penetrate the NF membrane into the permeate [1,30].

Table 3
Size distribution of three foulants at the variant ionic strength

	Mean diameter (nm, %Pd*)		
	5:5 mM	20:20 mM	50:50 mM
BSA	7.3 (17.2%)	10.4 (33.3%)	9.8 (55%)
HA	1.3 (20.1%)	1.6 (48.4%)	1.6 (37.4%)
BSA-HA	12.8 (18.3%)	12.1 (84%)	7.1 (52.4%)

*%Pd: volume particles distribution

Table 4
Contact angles of organic substances at different ionic strength

	Water (°) (I.S.)	Ethylene glycol (°)*	Diiodomethane (°)*	Zeta (mV)*
	82.1 ± 1.5 (5:5)			
BSA	79.1 ± 2.1 (20:20)	45.9 ± 3.7	51.2 ± 3.1	–4.7 ± 0.2
	50.7 ± 2.7 (50:50)			
	66.2 ± 1.0 (5:5)			
HA	61.9 ± 1.9 (20:20)	32.6 ± 0.4	56.1 ± 0.9	–27.3 ± 2.1
	55.5 ± 1.2 (50:50)			
	71.8 ± 4.5 (5:5)			
BSA-HA	82.0 ± 1.4 (20:20)	45.2 ± 2.0	52.7 ± 0.8	–9.6 ± 0.4
	60.8 ± 2.7 (50:50)			

*The probe was stayed at the same condition.

Table 5
Contact angles of NF membranes at different ionic strength

Membrane	I.S. (mM)	Water (°)	Ethylene glycol (°)	Diiodomethane (°)
	5:5	42.0 ± 1.2		
Virgin	20:20	45.1 ± 1.3	31.3 ± 0.8*	43.7 ± 0.7*
	50:50	46.1 ± 1.3		
	5:5	76.2 ± 4.0	67.4 ± 4.6	53.7 ± 0.9
BSA fouled	20:20	81.3 ± 1.2	51.5 ± 4.0	51.3 ± 3.2
	50:50	84.3 ± 0.5	51.6 ± 3.1	47.3 ± 1.6
	5:5	71.7 ± 3.7	39.7 ± 1.2	50.4 ± 2.4
HA fouled	20:20	63.5 ± 2.5	33.6 ± 2.3	54.3 ± 0.9
	50:50	47.0 ± 2.7	32.9 ± 0.6	56.9 ± 1.4
	5:5	85.2 ± 0.9	54.3 ± 1.9	50.3 ± 0.9
BSA-HA fouled	20:20	79.9 ± 3.3	59.3 ± 0.3	54.3 ± 0.8
	50:50	75.8 ± 4.3	50.0 ± 2.9	51.7 ± 0.3

*The probe was stayed at the same condition.

Table 6
Interfacial free energy for the permeate flux reduction at different ionic strength

Foulant	I.S. (mM)	G^{T}_{V} (mJ/m²)	G^{T}_{F} (mJ/m²)	J/J_0
BSA system	5:5	–31.1 ± 1.9	–42.0 ± 2.9	0.88
	20:20	–31.0 ± 0.4	–51.3 ± 2.1	0.79
	50:50	–24.3 ± 0.5	–51.6 ± 1.7	0.78
HA system	5:5	–20.2 ± 1.5	–26.4 ± 0.5	0.92
	20:20	–20.7 ± 0.8	–24.4 ± 0.4	0.87
	50:50	–13.9 ± 0.5	–11.5 ± 1.1	0.89
BSA-HA system	5:5	–25.6 ± 1.0	–44.0 ± 1.3	0.79
	20:20	–35.6 ± 2.4	–51.4 ± 3.6	0.69
	50:50	–27.7 ± 0.5	–31.3 ± 1.8	0.90

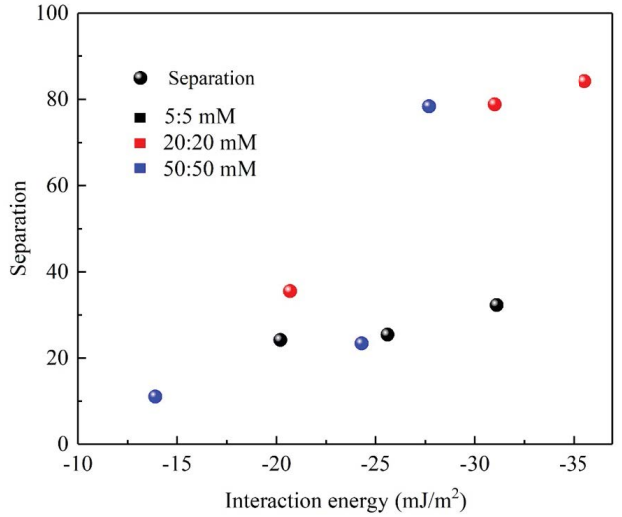

Fig. 5. Effect of interfacial free energy on ion separation on the virgin membrane at different ionic strength.

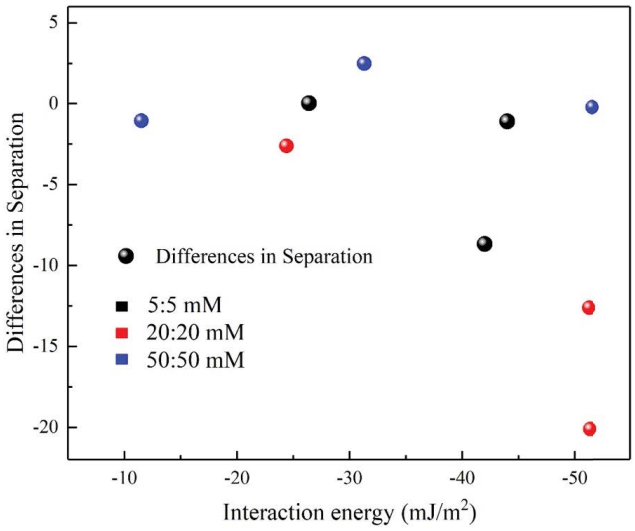

Fig. 6. Differences in separation of interfacial free energy on the fouled membrane at different ionic strength.

Fig. 6 illustrates the free energies of BSA, HA, and BSA-HA fouled membranes. The results demonstrate a positive correlation between the differences in ion separation degree (DIS) and the reduction in interfacial free energy at the end of fouling tests. As the G^{T}_{F} values decrease, there is a decrease in flux and a reduction in ions separation efficiency [31]. This phenomenon can be explained by two factors: (1) cake-enhanced concentration polarization, which is caused by hindered back-diffusion of salt ions and altered cross-flow hydrodynamics within the organic foulant deposit layers, leading to an enhanced salt concentration polarization layer [32], and (2) weakened electrostatic repulsive forces between Cl^{-}/SO_4^{2-} ions and the fouled membrane, attributed to the higher zeta potential value of foulants absorbed on the membrane surface [33].

4. Conclusion

Nanofiltration has several significant advantages, including high permeate flux and efficient separation of NaCl and Na_2SO_4. This study investigated the mutual influence between variant organic foulants and ionic strength based on the M-XDLVO theory, using both single foulants (BSA, HA) and a hybrid foulant (BSA-HA). For the virgin NF, lower interfacial energy foulants demonstrated improved ion separation due to the Donnan-like effect. Within the G^{T}_{V} range of –13.9 ± 0.5 mJ/m² and –35.6 ± 2.4 mJ/m², ion separation increased from 11.08 to 84.2. However, as fouling behavior worsened, the differences of ion separation in the lower interfacial energy was ten times the values of those in the higher interfacial energy, due to cake-enhanced concentration polarization and weakened electrostatic repulsive forces.

References

[1] M.D. Afonso, G. Hagmeyer, R. Gimbel, Streaming potential measurements to assess the variation of nanofiltration membranes surface charge with the concentration of salt solutions, Sep. Purif. Technol., 22–23 (2001) 529–541.
[2] D. Rall, D. Menne, A.M. Schweidtmann, J. Kamp, L. von Kolzenberg, A. Mitsos, M. Wessling, Rational design of ion separation membranes, J. Membr. Sci., 569 (2019) 209–219.
[3] S. Chakrabortty, J. Nayak, P. Pal, R. Kumar, P. Chakraborty, Separation of COD, sulphate and chloride from pharmaceutical wastewater using membrane integrated system: transport modeling towards scale-up, J. Environ. Chem. Eng., 8 (2020) 104275, doi: 10.1016/j.jece.2020.104275.
[4] A. Pérez-González, R. Ibáñez, P. Gómez, A.M. Urtiaga, I. Ortiz, J.A. Irabien, Nanofiltration separation of polyvalent and monovalent anions in desalination brines, J. Membr. Sci., 473 (2015) 16–27.
[5] N. Kabay, H. Kahveci, Ö. İpek, M. Yüksel, Separation of monovalent and divalent ions from ternary mixtures by electrodialysis, Desalination, 198 (2006) 74–83.
[6] P. Srimuk, X. Su, J. Yoon, D. Aurbach, V. Presser, Charge-transfer materials for electrochemical water desalination, ion separation and the recovery of elements, Nat. Rev. Mater., 5 (2020) 517–538.
[7] H. Zhang, Q. He, J. Luo, Y. Wan, S.B. Darling, Sharpening nanofiltration: strategies for enhanced membrane selectivity, ACS Appl. Mater. Interfaces, 12 (2020) 39948–39966.
[8] A.I. Cavaco Morão, A. Szymczyk, P. Fievet, A.M. Brites Alves, Modelling the separation by nanofiltration of a multi-ionic solution relevant to an industrial process, J. Membr. Sci., 322 (2008) 320–330.

[9] Z. Chen, Z. Li, J. Chen, P. Kallem, F. Banat, H. Qiu, Recent advances in selective separation technologies of rare earth elements: a review, J. Environ. Chem. Eng., 10 (2022) 107104, doi: 10.1016/j.jece.2021.107104.
[10] K.L. Jones, C.R. O'Melia, Protein and humic acid adsorption onto hydrophilic membrane surfaces: effects of pH and ionic strength, J. Membr. Sci., 165 (2000) 31–46.
[11] R. Chan, V. Chen, The effects of electrolyte concentration and pH on protein aggregation and deposition: critical flux and constant flux membrane filtration, J. Membr. Sci., 185 (2001) 177–192.
[12] X.-L. Wang, W.-N. Wang, D.-X. Wang, Experimental investigation on separation performance of nanofiltration membranes for inorganic electrolyte solutions, Desalination, 145 (2002) 115–122.
[13] S. Bason, V. Freger, Phenomenological analysis of transport of mono- and divalent ions in nanofiltration, J. Membr. Sci., 360 (2010) 389–396.
[14] B. Van der Bruggen, L. Braeken, Comparison of methods to enhance separation characteristics in nanofiltration, Ind. Eng. Chem. Res., 46 (2007) 2236–2242.
[15] C.-H. Tu, H.-L. Wang, X.-L. Wang, Study on transmembrane electrical potential of nanofiltration membranes in KCl and $MgCl_2$ solutions, Langmuir, 26 (2010) 17656–17664.
[16] C.Y. Tang, Y.-N. Kwon, J.O. Leckie, Fouling of reverse osmosis and nanofiltration membranes by humic acid—effects of solution composition and hydrodynamic conditions, J. Membr. Sci., 290 (2007) 86–94.
[17] Y.-N. Wang, C.Y. Tang, Fouling of nanofiltration, reverse osmosis, and ultrafiltration membranes by protein mixtures: the role of inter-foulant-species interaction, Environ. Sci. Technol., 45 (2011) 6373–6379.
[18] H. Mo, K.G. Tay, H.Y. Ng, Fouling of reverse osmosis membrane by protein (BSA): effects of pH, calcium, magnesium, ionic strength and temperature, J. Membr. Sci., 315 (2008) 28–35.
[19] W. Jiang, Y. Wei, X. Gao, C. Gao, Y. Wang, An innovative backwash cleaning technique for NF membrane in groundwater desalination: fouling reversibility and cleaning without chemical detergent, Desalination, 359 (2015) 26–36.
[20] I. Koyuncu, A. Lüttge, M.R. Wiesner, Interferometric observations and kinetic modeling of the chemical cleaning of humic materials deposited on membranes, J. Membr. Sci., 313 (2008) 127–134.
[21] W.S. Ang, A. Tiraferri, K.L. Chen, M. Elimelech, Fouling and cleaning of RO membranes fouled by mixtures of organic foulants simulating wastewater effluent, J. Membr. Sci., 376 (2011) 196–206.
[22] M.M. Motsa, B.B. Mamba, A.R.D. Verliefde, Combined colloidal and organic fouling of FO membranes: the influence of foulant–foulant interactions and ionic strength, J. Membr. Sci., 493 (2015) 539–548.
[23] A.S. Al-Amoudi, Factors affecting natural organic matter (NOM) and scaling fouling in NF membranes: a review, Desalination, 259 (2010) 1–10.
[24] J. Wei, C. Qiu, Y.-N. Wang, R. Wang, C.Y. Tang, Comparison of NF-like and RO-like thin film composite osmotically-driven membranes—implications for membrane selection and process optimization, J. Membr. Sci., 427 (2013) 460–471.
[25] A.L. Ahmad, N.H. Mat Yasin, C.J.C. Derek, J.K. Lim, Harvesting of microalgal biomass using MF membrane: kinetic model, CDE model and extended DLVO theory, J. Membr. Sci., 446 (2013) 341–349.
[26] F. Zhao, K. Xu, H. Ren, L. Ding, J. Geng, Y. Zhang, Combined effects of organic matter and calcium on biofouling of nanofiltration membranes, J. Membr. Sci., 486 (2015) 177–188.
[27] J.M. Thwala, M. Li, M.C.Y. Wong, S. Kang, E.M.V. Hoek, B.B. Mamba, Bacteria–polymeric membrane interactions: atomic force microscopy and XDLVO predictions, Langmuir, 29 (2013) 13773–13782.
[28] T. Lin, Z. Lu, W. Chen, Interaction mechanisms of humic acid combined with calcium ions on membrane fouling at different conditions in an ultrafiltration system, Desalination, 357 (2015) 26–35.
[29] R. Levenstein, D. Hasson, R. Semiat, Utilization of the Donnan effect for improving electrolyte separation with nanofiltration membranes, J. Membr. Sci., 116 (1996) 77–92.
[30] J. Gilron, N. Gara, O. Kedem, Experimental analysis of negative salt rejection in nanofiltration membranes, J. Membr. Sci., 185 (2001) 223–236.
[31] E.M.V. Hoek, M. Elimelech, Cake-enhanced concentration polarization: a new fouling mechanism for salt-rejecting membranes, Environ. Sci. Technol., 37 (2003) 5581–5588.
[32] P. Montes, J.A. Trejo González, M.E. Araoz, G.L. Iglesias, R.M. Trujillo, R.E. Madrid, A.M. Avila, Renewable carbon-based materials for enhanced ion concentration polarization in sustainable separation devices, J. Environ. Chem. Eng., 8 (2020) 104001, doi: 10.1016/j.jece.2020.104001.
[33] R. Hu, Y. He, C. Zhang, R. Zhang, J. Li, H. Zhu, Graphene oxide-embedded polyamide nanofiltration membranes for selective ion separation, J. Mater. Chem. A, 5 (2017) 25632–25640.